Ionospheric Variations Induced by Thunderstorms in the Central Region of Argentina during the RELAMPAGO-CACTI campaign

Constanza I. Villagrán Asiares *, M. Gabriela Nicora, Amalia Meza, María Paula Paula Natali, Eldo E. Ávila, Marcos Rubinstein, Farhad Rachidi

Posted Date: 27 July 2023

doi: 10.20944/preprints202307.1909.v1

Keywords: Thunderstorm; Ionosphere; Atmospheric Gravity Waves; RELAMPAGO-CACTI

Article

Ionospheric Variations Induced by Thunderstorms in the Central Region of Argentina during the RELAMPAGO-CACTI Campaign

Constanza I. Villagrán Asiares [1,2,3,4,*,†,‡], M. Gabriela Nicora [1,2,3,4,‡], Amalia Meza [1,4,5,‡], M. Paula Natali [1,4,5,‡], Eldo E. Ávila [6,‡], Marcos Rubinstein [7], and Farhad Rachidi [8]

1 National Council for Scientific and Technical Research (CONICET), Godoy Cruz 2290, Capital Federal,C1425FQB, Buenos Aires, Argentina
2 Center for Research in Lasers and Applications, UNIDEF (CITEDEF-CONICET), San Juan Bautista de La Salle 4397, Villa Martelli, B1603ALO, Buenos Aires, Argentina; gabriela@blueplanet.com.ar
3 French-Argentine Institute for Climate Studies and its Impacts (UMI-IFAECI-CNRS 3351) , Intendente Güiraldes 2160, Ciudad Universitaria Pabellón II - 2do. piso, Buenos Aires, C1428EGA, Argentina
4 School of Astronomy and Geophysics (FCAG-UNLP), Paseo del Bosque s/n, La Plata, Buenos Aires, B1900FWA, Argentina;villagranasiares.constanza@gmail.com
5 Laboratory MAGGIA - FCAG - UNLP, Paseo del Bosque s/n, La Plata, Buenos Aires, B1900FWA, Argentina; amaliameza@gmail.com, and mariapaulanatali@gmail.com
6 School of Mathematics, Astronomy and Physics, National University of Córdoba, IFEG-CONICET, Av. Medina Allende s/n, Ciudad Universitaria, Córdoba, X5000HUA, Argentina; eldoavila@gmail.com
7 IICT Institute, School of Engineering and Management Vaud, HES-SO University of Applied Sciences and Arts Western Switzerland,1401 Yverdon-les-Bains, Switzerland; marcos.rubinstein@heig-vd.ch
8 Electromagnetic Compatibility Laboratory, Swiss Federal Institute of Technology (EPFL), 1015 Lausanne, Switzerland; farhad.rachidi@epfl.ch
* Correspondence: villagranasiares.constanza@gmail.com; cvillagran@fcaglp.fcaglp.unlp.edu.ar;
‡ These authors contributed equally to this work.

Abstract: This study investigates the ionospheric variations resulting from thunderstorms that occurred between 00:00 UTC and 08:00 UTC on November 10, 2018, in the central region of Argentina, site of the RELAMPAGO-CACTI Project (Remote sensing of Electrification, Lightning, and Mesoscale/microscale Processes with Adaptive Ground Observations; Clouds, Aerosols, and Complex Terrain Interactions). The data used were the Total Electron Content (TEC), which was computed from Global Navigation Satellite System (GNSS) measurements provided by the Argentinian Continuous Satellite Monitoring Network (RAMSAC by its Spanish acronym) stations and the atmospheric electrical activity data that were provided by the Earth Networks Total Lightning Network (ENTLN). We observed that the generated disturbances have periods less than or equal to 100 minutes and peak-to-peak DVTEC amplitude values reaching up to 1.35 TECU (1 Total electron content unit $= 10^{16} electrons/m^2$). We also noted that these atmospheric gravity waves, which show the highest peak-to-peak amplitudes, occur during periods of intense lightning activity. Finally, we found that for a day with Atmospheric Electrical Activity (AEA), the peak-to-peak amplitudes of the waves are approximately 2.91 times greater than the peak-to-peak amplitudes of a day without AEA.

Keywords: thunderstorm; ionosphere; Atmospheric Gravity Waves; RELAMPAGO-CACTI

1. Introduction

The ionosphere is the region of the atmosphere constituted by the presence of ions and free electrons. It extends mainly between 60 km and 1000 km ([1]), and solar radiation is its principal ionization agent ([2]). Through Global Navigation Satellite System (GNSS) measurements, the total electron content (TEC) can be calculated. TEC is defined as the integrated electron density along the signal path from the satellite to the GNSS receiver ([3]). This can be dynamically perturbed by external influences, such as solar activity and, geomagnetic storms, among others; and by internal influences,

such as thunderstorms, earthquakes, etc. ([4]). Regarding internal influences, thunderstorms, and convective systems can generate wave structures in the ionospheric plasma ([3,5,6]). These structures, known as Atmospheric Gravity Waves (AGWs), have been related to electromagnetic pulses during thunderstorms ([7]), and they can also be detected by GNSS measurements ([8]). Overshooting top, lightning, or a combination of both can generate gravity waves ([3,9]). Transient Luminous Events (TLEs) and discharges originating in the stratiform region could be a source of these waves ([10,11]). AGWs can propagate vertically upwards and transfer energy and momentum to the ionosphere ([1]). As they ascend, they can become unstable and break up, generating secondary waves ([12]). These secondary waves on their journey modulate the ionospheric plasma in the E region ([12]). Models of AGWs originating from thunderstorms predict variations in TEC of 7% ([13]). In [14], AGWs with periodicities between 25 to 30 minutes and peak-to-peak amplitudes greater than 0.3 TECU were found. In addition, waves with periodicities less than 4 minutes and peak-to-peak amplitudes around 0.1 TECU, known as Acoustic waves, were also detected. Both were observed in the central region of Argentina. Therefore, considering these investigations and continuing with the research carried out by [14], we aim to study the ionospheric variations generated by thunderstorms that developed in central Argentina, focusing on the amplitude and periodicity of AGWs and their horizontal range with respect to the center of the storms.

The north-central region of Argentina is a zone of the world with a high frequency of severe weather reports, such as hail, flooding, tornadoes, and strong wind gusts ([15–17]). On November 22, 2018, accumulated precipitation exceeding 200 mm was recorded in northern Argentina and Paraguay, caused by a mesoscale convective system ([18]). Hailstones of 4 cm has also been recorded over the province of Mendoza ([19]) and greater than 15 cm in Villa Carlos Paz, province of Córdoba, Argentina ([20,21]). The Remote Sensing of Electrification, Lightning, and Mesoscale/Microscale Processes with Adaptive Ground Observations (RELAMPAGO; [22]); and the Cloud, Aerosol, and Complex Terrain Interactions (CACTI; [23]) (RELAMPAGO-CACTI, [24]) projects were conducted in late 2018 and mid-April 2019 in order to study the convective storms that produce these high-impact meteorological events, often along the Sierras de Córdoba and the Andes. These projects were implemented in the provinces of Córdoba and Mendoza in Argentina and western Rio Grande do Sul in Brazil. More than 200 researchers from the United States, Brazil, and Argentina participated in the RELAMPAGO-CACTI campaign. The location and timing of the RELAMPAGO - CACTI project were chosen as the ideal scenario for this study.

The paper is divided into five sections. Section 2 describes the data used and the methodology employed. Sections 3 and 4 present results and discussion, respectively. Finally, Section 5 is devoted to the conclusions.

2. Materials and Methods

As mentioned above, solar activity plays a significant role in the ionization process of the upper atmosphere. We worked during nighttime to reduce these effects on geomagnetically quiet days, with planetary index $K_p < 4$, [25]. K_p describes the average level of irregularities in the horizontal components of the Earth's magnetic field ([1]). Thus, during the analysis period, 00:00 UTC – 08:00 UTC (21:00 LT - 05:00 LT), two days of 2018 with $K_p \leq 2$ were selected. November 10, with some electrical activity detected, and September 9, without lightning. We worked in the region defined between latitudes 64°S – 21°S and longitudes 80°W – 53°W, as can be seen in Figure 1.

Preprints (www.preprints.org) | NOT PEER-REVIEWED | Posted: 27 July 2023 doi:10.20944/preprints202307.1909.v1

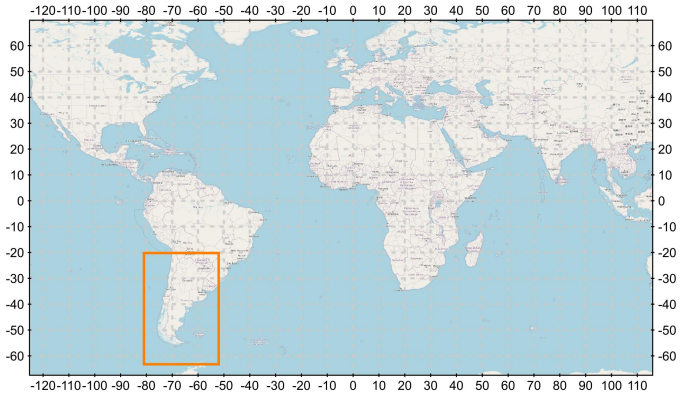

Figure 1. Study region outlined in orange.

The data used in this paper are:

- Atmospheric Electrical Activity (AEA) data detected by the Earth Networks Total Lightning Network (ENTLN) [26]. ENTLN uses broadband sensors with frequencies between 1 Hz - 12 MHz. ENTLN can distinguish between the type of discharge, i.e. Cloud-to-Ground (CG) and In-Cloud (IC) lightning. This network consists of more than 1800 sensors deployed in more than 100 countries ([27]). There are 50 sensors installed in Argentina. The sensors record the electric field signals produced by lightning, which are sent to the central processor. Using the time-of-arrival (TOA) technique, the lightning is geolocated in real time ([27]). The data obtained from this network are the type of discharge (CG or IC), the time of occurrence, the geolocation, the estimated peak current, the height of the detected IC discharge, the multiplicity of the discharges, and the number of sensors that detected the discharge. More information can be found in [28].
- Advanced Baseline Imaging (ABI) data from the GOES-R 16 series of Geostationary Operational Environmental Satellites (GOES) corresponding to channel 13, wavelength 10.3 μm. The data are free and available at [29]. Detailed information on GOES-16 and the ABI sensor can be found in [30].
- GNSS observation data from the Crustal dynamics data information system (CDDIS), [31], and the Argentine Continuous Satellite Monitoring Network (RAMSAC, [32]). Figure 2 shows the RAMSAC Stations used in this study.

In order to analyze the ionospheric variations generated by thunderstorms, the following procedure was carried out. First, we used the cloud-top Brightness Temperature (BT), corresponding to channel 13, wavelength 10.3 μm of the GOES-R 16 satellite, as a proxy for the optically thick cloud-top temperature ([33]). Radiation at this wavelength (10.3 μm) is not affected by absorption by atmospheric gases ([34]). Using cloud-top Brightness Temperature (BT) and thunderstorm discharge data, the temporal evolution of thunderstorms on November 10, 2018, was studied. Statistical and descriptive analyzes of the lightning detected were then performed. The analyzed parameters were the peak current and the lightning count. "The lightning count is the number of lightning events that occurred" ([35]). In addition, we classified the lightning strokes according to their type (i.e., CG and IC) and polarity (i.e., negative or positive).

Preprints (www.preprints.org) | NOT PEER-REVIEWED | Posted: 27 July 2023 doi:10.20944/preprints202307.1909.v1

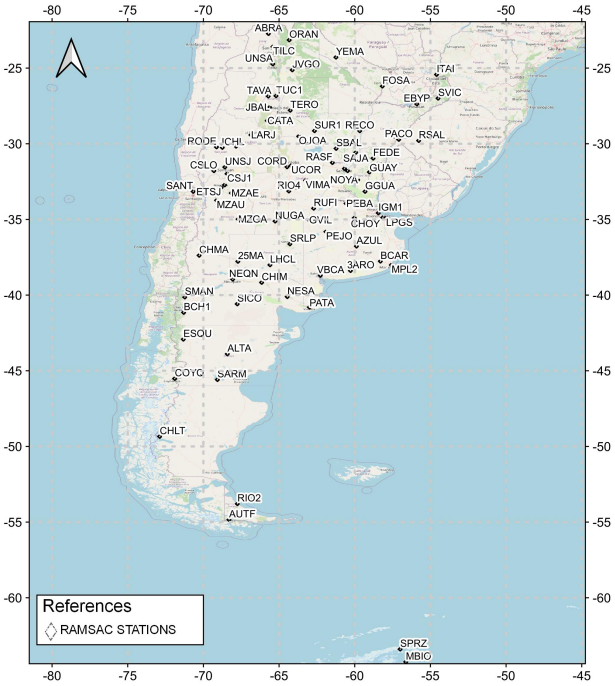

Figure 2. RAMSAC Stations [32].

The GNSS data were then preprocessed with Bernese GNSS software version 5.2 ([36]). This software uses the models recommended by the International Earth Rotation and Reference Systems Service (IERSS) ([37]). These models include ocean and atmospheric tidal loading corrections ([38,39]) and absolute phase-center corrections for satellites and receivers from IGS. The phase-code delay ionospheric observable along with the geographic latitude and the sun–fixed longitude of the ionospheric pierce point, zenith distance (z'), azimuth angle, and time for each satellite over each GNSS station was obtained. Subsequently, for September 9 and November 10, 2018, the Vertical Total Electron Content (VTEC) was obtained using a program developed by MAGGIA Laboratory (Meteorología espacial, Atmósfera terrestre, Geodesia, Geodinámica, desarrollo de instrumentos y Astrometría; [40]) ([41,42]). The ionosphere was approximated by a single shell of infinitesimal thickness with equivalent total oblique electron content (STEC), located 450 km above the Earth's surface. An obliquity factor, $1/cos(z')$, was used to convert STEC measurements to VTEC:

$$STEC = VTEC * \frac{1}{cos(z')} \tag{1}$$

where z' is the zenith distance of the oblique path at the ionospheric piercing point (IPP). For this work, $z' \geq 30^{o}$ was used. The ionospheric code delay observable was modeled using the procedure explained in ([41,42]). Finally, VTEC measurements in each station were detrended using a 6th to 7th order polynomial fit ([3]). The previous process removes the gross offset, as well as the trend value obtaining Differential Vertical Total Electron Content (DVTEC) values. The remaining variability is mainly related to the carrier phase, whose accuracy is 0.01 to 0.1 TECU [43].

Once the DVTEC was obtained, its peak-to-peak amplitude was calculated, using the following definition:

$$peak - to - peak - Amplitude = maxDVTEC - minDVTEC. \tag{2}$$

where $maxDVTEC$ and $minDVTEC$ are the maximum and minimum values of DVTEC, respectively.

Finally, the C-Morlet 1.5 wavelet transform was used to analyze the spectral amplitude and period of the DVTEC signal ([44]).

Preprints (www.preprints.org) | NOT PEER-REVIEWED | Posted: 27 July 2023 doi:10.20944/preprints202307.1909.v1

3. Results

This section is divided into three parts. The electrical characterization and analysis of DVTEC variations on November 10, 2018, are presented in the first and second parts,respectively. In the third part, a comparison of DVTEC variations between November 10 and September 9, 2018 (day without electrical activity) is made.

3.1. Characterization of the Atmospheric Electrical Activity

Within the study region, on November 10, 2018, two thunderstorms are observed in the subregion defined between latitudes 43ºS - 28ºS and longitudes 70ºW - 51ºW (yellow box in Figure 3). The storm cell located in the central region started at 23:00 UTC, and the storm cell located in the southeast started at 16:00 UTC on November 9, 2018, both cells with southeastward motion. Around 04:00 UTC on November 10, 2018, both storms merged into a large system. They reached their dissipation stage at around 16 UTC on that day. Their dissipation stage was short-lived, due to the generation of other storms that merged with them. During the selected analysis period, from 00:00 UTC to 08:00 UTC, the storm cells reached cloud tops below -70°C, which suggests that the storms achieved their maximum vertical development. This is shown in Figure 3, where the color bar illustrates the range of brightness temperatures (BT). The colder colors correspond to BT values ranging between -60°C and -40°C, while the warmer colors represent BT below -80°C to -70°C. The gray to black colors indicate BT between -90°C and -80°C. Zones of deep convection would be delineated by warm colors and colors ranging from gray to black.

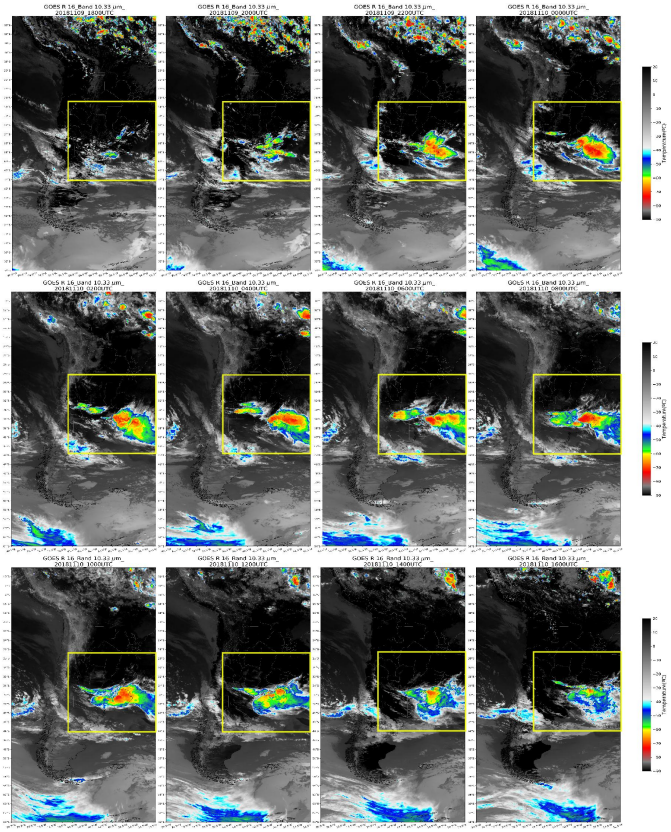

Figure 3. GOES-R 16 image, channel 13 (10.3 μm). Plots are made every two hours from 18:00 UTC on November 9, 2018 to 16:00 UTC on November 10, 2018. The study subregion, defined between latitudes 43ºS - 28ºS and longitudes 70ºW - 51ºW, is outlined in yellow.

During the night of November 10, between 00:00 UTC and 08:00 UTC, a total of 128,939 discharges were recorded, with 40% being -IC (negative intra-cloud) and 3% being +CG (positive cloud-to-ground).

Preprints (www.preprints.org) | NOT PEER-REVIEWED | Posted: 27 July 2023 doi:10.20944/preprints202307.1909.v1

Figures 4 and 5 depict the detected lightning discharges at a given moment. The graphics classify the discharges based on type and polarity as follows: positive +CG (light blue star) and +IC (brown diamond); negative -CG (blue star) and -IC (green diamond). By examining the images, it can be observed that during these time intervals, the majority of the recorded discharges are associated with $BT \leq -70C$ indicating their proximity to deep convective zones.

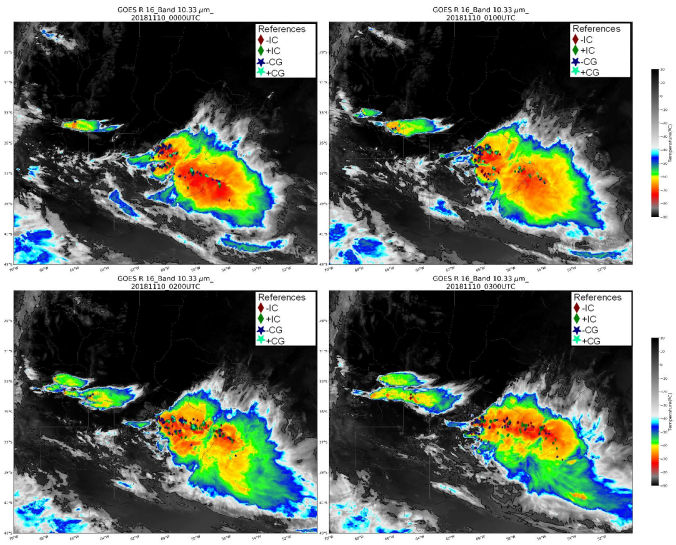

Figure 4. Evolution of hourly storms from 00:00 UTC to 03:00 UTC in the study subregion. Diamonds are used to represent IntraCloud (IC) discharges (brown for -IC and green for +IC), and stars to represent Cloud-to-Ground (CG) discharges (blue for -CG and light blue for +CG). The color scale represents the brightness temperature corresponding to band 13 of the ABI sensor, GOES-R 16.

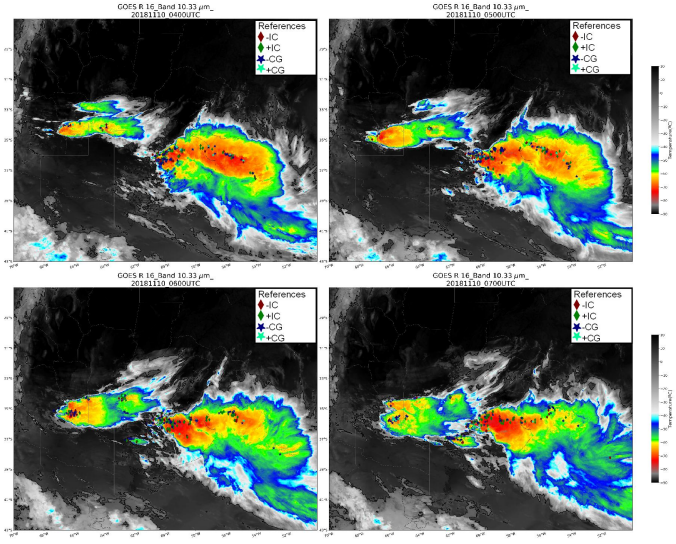

Figure 5. Evolution of hourly storms from 04:00 UTC to 07:00 UTC in the study subregion. Diamonds are used to represent IntraCloud (IC) discharges (brown for -IC and green for +IC), and stars to represent Cloud-to-Ground (CG) discharges (blue for -CG and light blue for +CG). The color scale represents the brightness temperature corresponding to band 13 of the ABI sensor, GOES-R 16.

Considering the estimated peak current of the discharges, we find that CG-type discharges exhibit maximum peak current values exceeding 200 kA, while IC-type discharges reach values around 30 kA (see Table 1). These peak currents are located over the regions of maximum lightning counts, which are observed in Figure 6. In that Figure, the lightning counts are spatially illustrated on a 0.2° by 0.2° grid,

Preprints (www.preprints.org) | NOT PEER-REVIEWED | Posted: 27 July 2023 doi:10.20944/preprints202307.1909.v1

where the light colors represent the locations with the highest counts. The highest lightning counts are found at the northwest end of the cell located in the southeast region, reaching values above 2290 discharges.

Table 1. Statistical table of estimated peak current from 00:00 UTC to 08:00 UTC (21:00 LT - 05:00 LT).

	Peak currents (kA)		
Types of discharges	**Average**	**Maximum**	**Minimum**
- IC	-9.55	-29.99	-1.69
+ IC	10.89	29.99	1.42
- CG	-16.46	-267.25	-3.50
+ CG	33.15	322.64	15.00

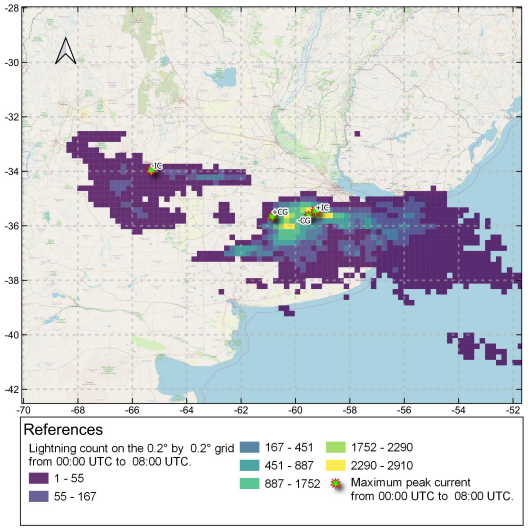

Figure 6. Lightning count on the 0.2º by 0.2º grid from 00:00 to 08:00 UTC (21:00 LT - 05:00 LT). Light colors represent the location with the highest lightning count. The stars indicate the sites where the maximum peak currents of the +CG, -CG, +IC, and -IC discharges occurred.

To analyze the temporal variation of discharges, we examined the distribution of relative frequencies of discharges per hour (left panel of Figure 7) and per time period (right panel of Figure 7). Dividing the discharges into time periods will allow us to investigate their relationship with the ionosphere, which will be analyzed in the next section. Looking at the graph on the left, we could recognize an increase in atmospheric electrical activity (AEA) during the early hours. Subsequently, a decrease was observed, followed by a new increase. In the graph on the right, we see that each one of the three periods contains than 30% of the discharges, the interval between 02:40 UTC and 05:20 UTC presenting the highest number of discharges, corresponding to more than 35%. Between 00:00 UTC - 02:40 UTC, 02:40 UTC - 05:20 UTC, and 05:20 UTC - 08:00 UTC more than 42000, 48000, and 38000 discharges are recorded, respectively. Overall, 70% of the events were reported as IC discharges and 30% as CG discharges. The highest number of detected discharges corresponds to -IC.

Preprints (www.preprints.org) | NOT PEER-REVIEWED | Posted: 27 July 2023 doi:10.20944/preprints202307.1909.v1

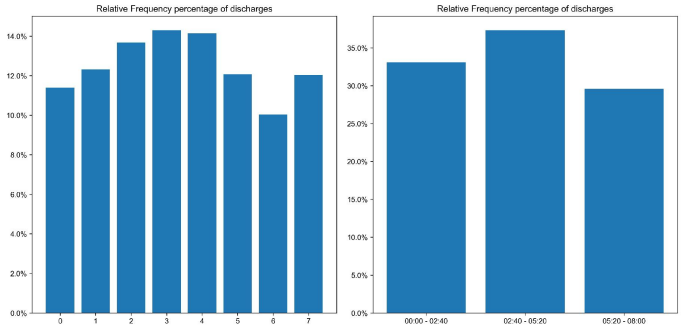

Figure 7. Right. Relative frequency of lightning at UTC hour. Left. Relative frequency of lightning at the period of time.

For each time period, the maximum, minimum, and average peak current is calculated and presented in Table 2. Looking at the Table, we see that the IC discharges present maximum peak current values close to 30 kA, and minimum values around 1.8 kA with mean values of 9 kA and 10 kA for the -IC and +IC discharges, respectively. On the other hand, CG discharges have peak current values above 200 kA, minimum values of 3.5 kA and 15.00 kA with mean values of 15 kA and 33 kA for -CG and +CG discharges, respectively. The table highlights in red the maximum values reached in each time period, which correspond to the CG discharges. The maximum peak occurred between 05:20 UTC - 08:00 UTC (02:20 LT - 05:00 LT).

Table 2. Statistical table of estimated peak current for each period of time.

UTC time period	Peak currents (kA)								
	00:00 - 02:40			02:40 - 05:20			05-:20 - 08:00		
Types of discharges	Avg	Max	Min	Avg	Max	Min	Avg	Max	Min
- IC	-9.8	-29.9	-2.2	-9.1	-29.9	-1.7	-9.8	-29.9	-1.7
+ IC	11.5	29.9	2.29	10.5	29.9	1.8	10.7	29.9	1.4
- CG	-15.8	-219.2	-3.5	-14.4	-214.13	-3.5	-20.2	-267.3	-3.5
+ CG	31.5	181.5	15.0	34.0	211.1	15.0	33.9	322.6	15.0

To identify the locations of the maximum estimated peak currents in each time period, we generated Figures 8, 9, and 10. These figures depict the same spatial distribution as Figure 6, but for different time periods. Looking at them, we see that between 00:00 UTC - 02:40 UTC and 05:20 UTC - 08:00 UTC the maximum peak current values for +IC, -CG and +CG are located over the most developed cell corresponding to the southeast storm, near the maximum lightning count. The maximum peak current for -IC is located during the period 00:00 UTC - 02:40 UTC over the least developed cell, corresponding to the central region storm. For the period 05:20 UTC - 08:00 UTC, it is located over the southeast storm, near the maximum lightning count. In contrast to the other time periods, between 02:40 UTC and 05:20 UTC, the maximum peak current values for +IC, -IC, -CG and +CG are located over the central region storm (see Figure 9), far from the area of highest lightning counts.

Preprints (www.preprints.org) | NOT PEER-REVIEWED | Posted: 27 July 2023 doi:10.20944/preprints202307.1909.v1

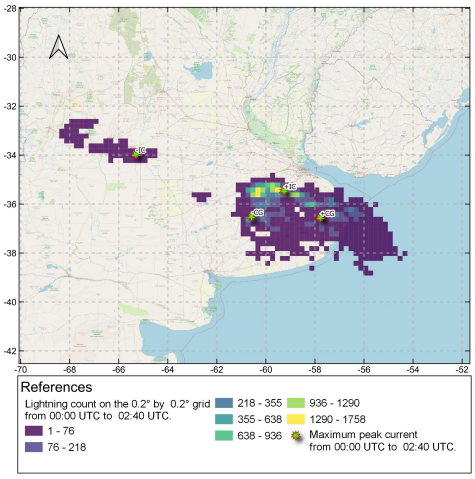

Figure 8. Lightning count on the 0.2º by 0.2º grid from 00:00 UTC to 02:40 UTC (21:00 LT - 23:40 LT). Light colors represent the location with the highest lightning count. Stars indicate the locations where the peak currents of the +CG, -CG, +IC, and -IC discharges occurred.

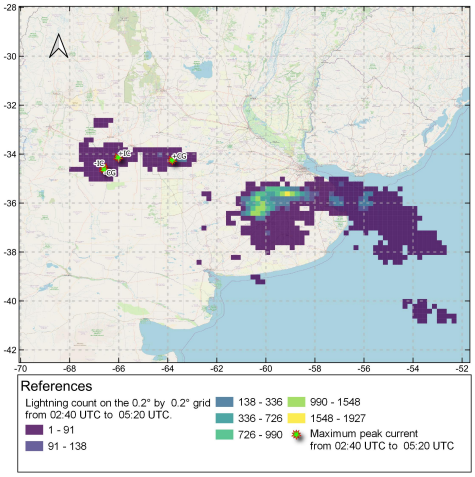

Figure 9. Lightning count on the 0.2º by 0.2º grid from 02:40 UTC to 05:20 UTC (23:40 LT - 02:20 LT). Light colors represent the location with the highest lightning count. Stars indicate the locations where the peak currents of the +CG, -CG, +IC, and -IC discharges occurred.

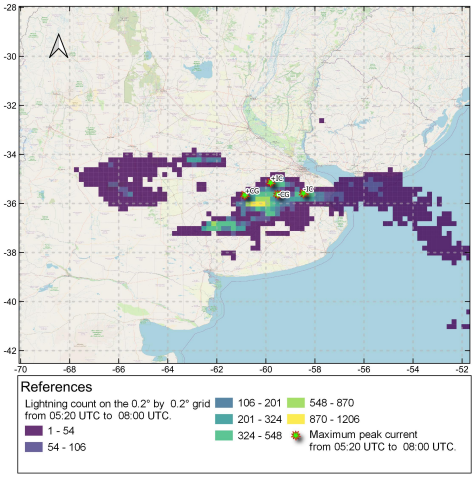

Figure 10. Lightning count on the 0.2º by 0.2º grid from 05:20 UTC to 08:00 UTC (02:20 LT - 05:00 LT). Light colors represent the location with the highest lightning count. Stars indicate the locations where the peak currents of the discharges +CG, -CG, +IC, and -IC occurred.

Preprints (www.preprints.org) | NOT PEER-REVIEWED | Posted: 27 July 2023 doi:10.20944/preprints202307.1909.v1

Summarizing,

- More than 70% of the discharges are of the IC type, mainly of negative polarity. This result is in agreement with the overall ratio given in the literature ,in which, although dependent on the type of storm, the latitude, and other parameters, CG discharges constitute overall 25% and IC discharges 75% of the atmospheric electrical activity (e.g., [45]).
- The highest peak currents are obtained for CG discharges, where the maximum peak corresponds to +CG discharges (322 kA), followed by -CG discharges (267 kA). Both occur between 05:20-08:00 UTC (02:20 LT - 05:00 LT). In this time period the average peak currents were 34 kA for +CG and 20 kA for -CG . These average peak current values are in agreement with the values found in [46], which for our study area ranges from 10 kA to 30 kA. Also the estimated average peak current (34 kA) is consistent with [47] data obtained using direct measurements.

3.2. Analysis of Ionospheric DVTEC Disturbances

In this section, we will analyze the DVTEC disturbances generated by the storm of 10 December 2018. Subsequently, we will make a comparison of the ionospheric response produced on this day, when Atmospheric Electrical Activity was present, with the ionospheric response of a day without electrical activity (9 September 2018). Finally, we will analyze the data by applying the wavelet transform to the DVTEC values.

3.2.1. DVTEC Variations Due to Thunderstorms

Three geographical zones were defined for analysis purposed as, illustrated in Figure 11. In addition, the figure shows the RAMSAC stations and the lightning counts as a grid of a 0.2° by 0.2° cells. The working zones represent:

- Zone 1: the thunderstorms region,
- Zone 2: the region around the thunderstorms and adjacent to it, and
- Zone 3: the area away from the thunderstorms.

Figures 12, 13 and 14 illustrate the variation of DVTEC on 10 November 2018 across multiple stations and GNSS satellites. These figures provide a visual representation of the DVTEC changes observed within the specified analysis zones. Results from each station are vertically offset from the previous station by 1 TECU $(10^{16} electrons/m^2)$. In each plot, the three time intervals defined in the previous section are marked with different colors in the horizontal axis in decimal time. The interval from 0 UTC to 2.66 UTC (i.e., 00:00 UTC - 02:40 UTC) is marked in blue, the interval from 2.66 UTC to 5.33 UTC (i.e., 02:40 UTC - 05:20 UTC) is marked in yellow, and the interval from 5.33 UTC to 8 UTC (i.e., 05:20 UTC - 08:00 UTC) is marked in green. Additionally, in each figure, the names of the stations exhibiting large deviations in DVTEC, with peak-to-peak amplitudes greater than 1 TECU, are highlighted in light blue in the vertical axis. Comparing Figures 12, 13, and 14, it is observed that the signals become progressively more unstable, especially in zone 3 (see Figure 14). Analyzing the temporal evolution of the signals within each zone, it is evident that the most significant magnitude variations occur during the interval from 02:40 UTC to 05:20 UTC, coinciding with the peak of thunderstorm electrical activity.

Preprints (www.preprints.org) | NOT PEER-REVIEWED | Posted: 27 July 2023 doi:10.20944/preprints202307.1909.v1

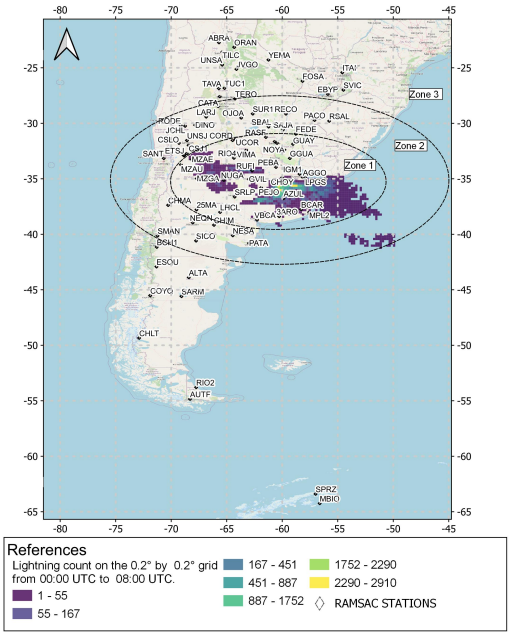

Figure 11. Lightning counts on the 0.2° by 0.2° grid from 00:00 UTC to 08:00 UTC (21:00 LT - 05:00 LT). Light colors represent locations with the highest lightning counts. RAMSAC stations are marked with diamonds, and the three study zones are delimited with ellipses.

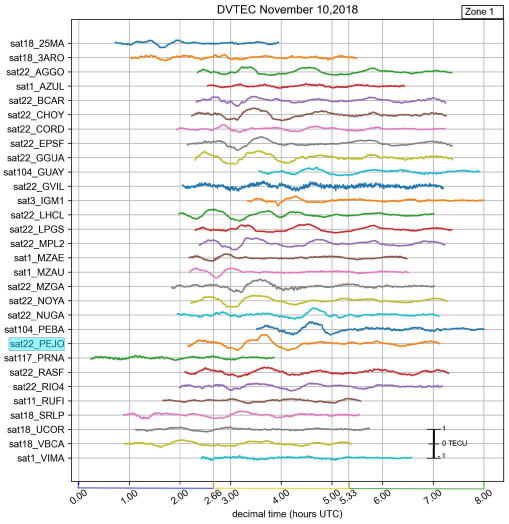

Figure 12. Temporal variations of the differential vertical total electron content (DVTEC) of the RAMSAC stations within Zone 1. On the x-axis, with colored bars, the three time periods analyzed in the previous section are represented, blue for the period 00:00 UTC- 02:40 UTC (i.e. 21:00 LT - 23:40 LT), yellow for the interval 02:40 UTC- 05:20 UTC (i.e. 23:40 LT- 02:20 LT), and in green for the period 05:20 UTC - 08:00 UTC (i.e. 02:20 LT - 05:00 LT). On the y-axis, the stations are located 1 TECU apart. A scale is shown in the figure as a reference. The stations with the largest deviations observed in DVTEC are outlined in blue.

Preprints (www.preprints.org) | NOT PEER-REVIEWED | Posted: 27 July 2023 doi:10.20944/preprints202307.1909.v1

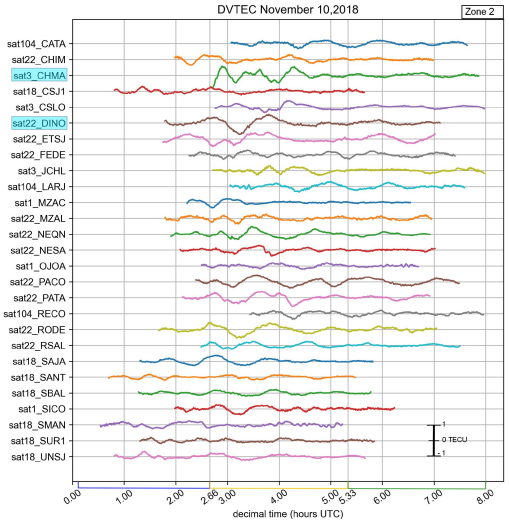

Figure 13. Temporal variations of the differential vertical total electron content (DVTEC) of the RAMSAC stations within Zone 2.On the x-axis, with colored bars, the three time periods analyzed in the previous section are represented, blue for the period 00:00 UTC- 02:40 UTC (i.e. 21:00 LT - 23:40 LT), yellow for the interval 02:40 UTC- 05:20 UTC (i.e. 23:40 LT- 02:20 LT), and in green for the period 05:20 UTC - 08:00 UTC (i.e. 02:20 LT - 05:00 LT). On the y-axis, the stations are located 1 TECU apart. A scale is shown in the figure as a reference. The stations with the largest deviations observed in DVTEC are outlined in blue.

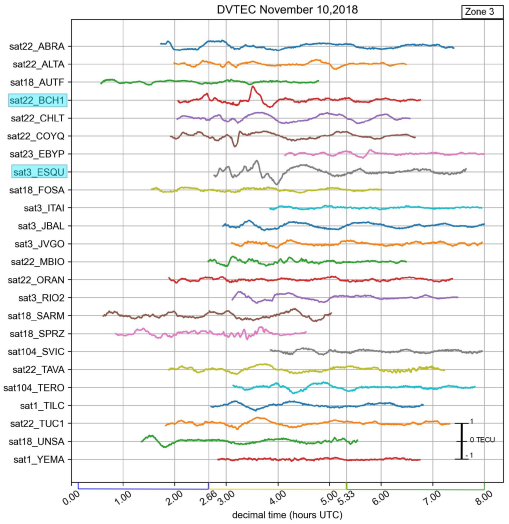

Figure 14. Temporal variations of the differential vertical total electron content (DVTEC) of the RAMSAC stations within Zone 3. On the x-axis, with colored bars, the three time periods analyzed in the previous section are represented, blue for the period 00:00 UTC- 02:40 UTC (i.e. 21:00 LT - 23:40 LT), yellow for the interval 02:40 UTC- 05:20 UTC (i.e. 23:40 LT- 02:20 LT), and in green for the period 05:20 UTC - 08:00 UTC (i.e. 02:20 LT - 05:00 LT). On the y-axis, the stations are located 1 TECU apart. A scale is shown in the figure as a reference. The stations with the largest deviations observed in DVTEC are outlined in blue.

The analysis performed showed that, the peak-to-peak amplitudes of the DVTEC variations are different for each station and satellite. Figures 15–17 present the positions of the RAMSAC stations and their respective peak-to-peak DVTEC amplitude ranges. The peak-to-peak amplitude ranges were calculated for each time interval, i.e., the peak-to-peak amplitude range corresponding to the period 00:00 UTC - 02:40 UTC is presented in the upper left panel, the amplitude range for the interval

Preprints (www.preprints.org) | NOT PEER-REVIEWED | Posted: 27 July 2023 doi:10.20944/preprints202307.1909.v1

02:40 UTC - 05:20 UTC in the upper right panel, and the range for 05:20 UTC - 08:00 UTC in the lower left panel. The figures also include the lightning counts plotted in the 0.2° by 0.2° grid for each of the analyzed time periods. Each station is represented by a diamond, whose color indicates the peak-to-peak DVTEC range measured at that station. The locations of the events reported by the Earth Networks system to have the maximum peak currents for the different discharge types are represented by stars.

In the period 00:00 UTC - 02:40 UTC (i.e., 21:00 LT - 23:40 LT), a predominance of peak-to-peak DVTEC amplitudes between 0.21 TECU and 0.44 TECU is observed in all three zones. In zones 1 and 2, peak-to-peak DVTEC amplitudes average 0.3 TECU, while in Zone 3, they average 0.22 TECU. In this time interval, peak-to-peak DVTEC amplitude values of up to 0.67 TECU are observed. In Zone 1, the peak-to-peak DVTEC amplitude maxima surround the storms; while in zones 2 and 3, the maxima are generally located in the western region of the country. Recall that, for this time period, the storm was in its growth phase.

Between 02:40 UTC - 05:20 UTC (i.e., 23:40 LT - 02:20 LT), a predominance of peak-to-peak DVTEC amplitudes between 0.44 TECU and 0.67 TECU is observed in all three zones. Average peak-to-peak DVTEC amplitudes of 0.61 TECU, 0.65 TECU and 0.57 TECU are obtained for zones 1, 2 and 3, respectively. Peak-to-peak DVTEC amplitude values of up to 1.11 TECU are observed for zone 1 and 1.35 TECU for zones 2 and 3. These maxima are located for zone 1 mainly between the storms (Figure 15); while for zones 2 and 3 (Figures 16 and 17) they are located over the mountain range. In this time period, the storms were in their development - maturity phase.

Finally, in the time interval 05:20 UTC - 08:00 UTC (02:20 LT - 05:00 LT), peak-to-peak DVTEC amplitude values of up to 0.67 TECU were observed, mainly located in the northern region of the country. Likewise, a predominant peak-to-peak DVTEC amplitude between 0.21 TECU and 0.44 TECU was observed. An average peak-to-peak DVTEC amplitude of 0.25 TECU for zones 1 and 3, and of 0.3 TECU for Zone 2 are also observed. During this time period, thunderstorm electrical activity was decreasing.

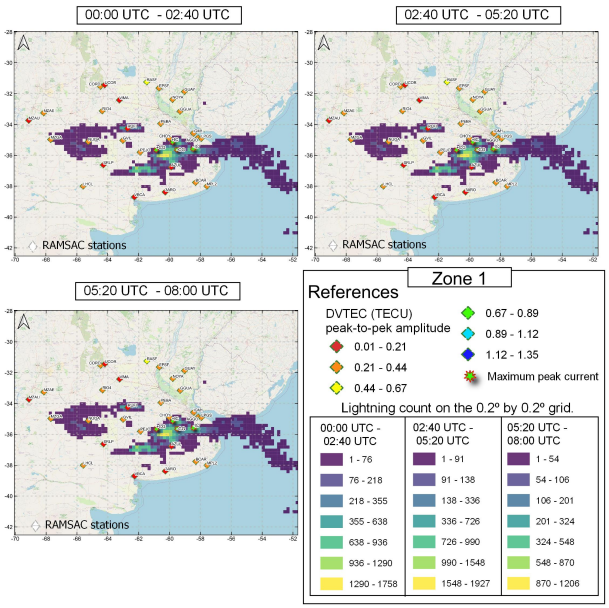

Figure 15. Map of RAMSAC stations in Zone 1. The range of peak-to-peak DVTEC amplitudes obtained at each station are marked with colored diamonds. Lightning counts are plotted on the 0.2° by 0.2° grid. Light colors represent the location with the highest lightning counts. The locations of the maximum peak currents for IC and CG discharges are indicated by stars. The three maps represent, the three time periods analyzed: top left map: 00:00 UTC - 02:40 UTC (21:00 LT - 23:40 LT); top right map: 02:40 UTC - 05:20 UTC (23:40 LT - 02:20 LT); bottom left map: 05:20 UTC - 08:00 UTC (02:20 LT - 05:00 LT).

Preprints (www.preprints.org) | NOT PEER-REVIEWED | Posted: 27 July 2023 doi:10.20944/preprints202307.1909.v1

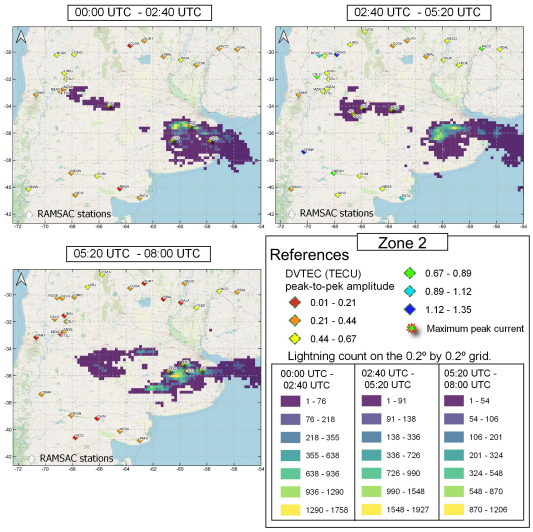

Figure 16. Map of RAMSAC stations in Zone 2. The range of peak-to-peak DVTEC amplitudes obtained at each station are marked with colored diamonds. Lightning counts are plotted on the 0.2° by 0.2° grid. Light colors represent the location with the highest lightning counts. The locations of the maximum peak currents for IC and CG discharges are indicated by stars. The three maps represent, the three time periods analyzed: top left map: 00:00 UTC - 02:40 UTC (21:00 LT - 23:40 LT); top right map: 02:40 UTC - 05:20 UTC (23:40 LT - 02:20 LT); bottom left map: 05:20 UTC - 08:00 UTC (02:20 LT - 05:00 LT).

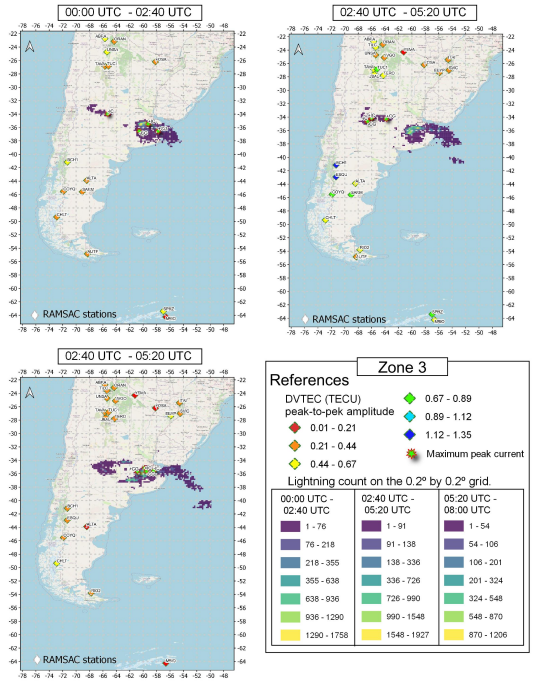

Figure 17. Map of RAMSAC stations in Zone 3. The range of peak-to-peak DVTEC amplitudes obtained at each station are marked with colored diamonds. Lightning counts are plotted on the 0.2° by 0.2° grid. Light colors represent the location with the highest lightning counts. The locations of the maximum peak currents for IC and CG discharges are indicated by stars. The three maps represent, the three time periods analyzed: top left map: 00:00 UTC - 02:40 UTC (21:00 LT - 23:40 LT); top right map: 02:40 UTC - 05:20 UTC (23:40 LT - 02:20 LT); bottom left map: 05:20 UTC - 08:00 UTC (02:20 LT - 05:00 LT).

Preprints (www.preprints.org) | NOT PEER-REVIEWED | Posted: 27 July 2023 doi:10.20944/preprints202307.1909.v1

3.2.2. Comparison with a Day without Storms

To analyze the ionospheric behavior during a thunderstorm, we chose a day in Argentina with no atmospheric electrical activity (AEA). We designated September 9, 2018 as the base day for comparative purposes. In this study, we chose 14 RAMSAC stations, whose distribution can be seen in Figure 18. The right image in the Figure represents the lightning counts on a 0.2° by 0.2° grid. The points where the peak current of the different types of discharges were reported to have occurred by the Earth Network system are marked with a star. From Figure 18, we observe that the RAMSAC stations are distributed as follows:

- six stations in Zone 1: AZUL, CHOY, CORD, MZGA, PEBA, SRLP;
- three stations from Zone 2: CHIM, SAJA, UNSJ; and
- five stations in Zone 3: ESQU, ORAN, RIO2, SVIC, TERO.

In addition, we can see that the AZUL and CHOY stations are the closest to the regions with the highest number of discharges. These stations, together with MZGA, are located near the highest current peaks. Note that SRLP and PEBA are located between the storms.

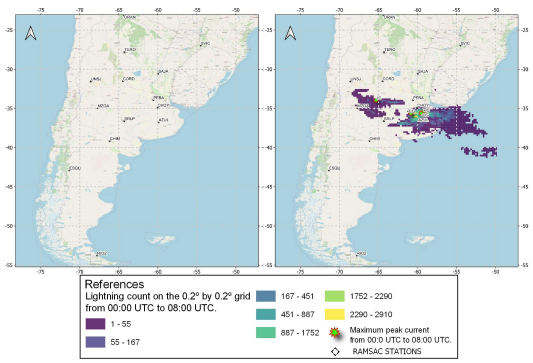

Figure 18. Maps of the 14 RAMSAC stations on September 9, reference day (left image), and on November 10, 2018, day with AEA (right image). On the November 10 map, lightning count is plotted on the 0.2º by 0.2º grid, and the locations where the highest current peaks occurred for intracloud (IC) and for Cloud-to-Ground (CG) discharges are indicated with stars.

When comparing the DVTEC variations between the two days (refer to Figures 19 and 20), it is evident that the day with AEA exhibits significant fluctuations in DVTEC. The stations with the highest variability are highlighted in light blue in Figure 20. Three of the stations, namely CHOY, MZGA, and PEBA, are situated in Zone 1, which corresponds to the storm region. Furthermore, the ESQU station also recorded considerable deviations in DVTEC, despite being located in Zone 3, specifically in the Andes mountain range.

Preprints (www.preprints.org) | NOT PEER-REVIEWED | Posted: 27 July 2023 doi:10.20944/preprints202307.1909.v1

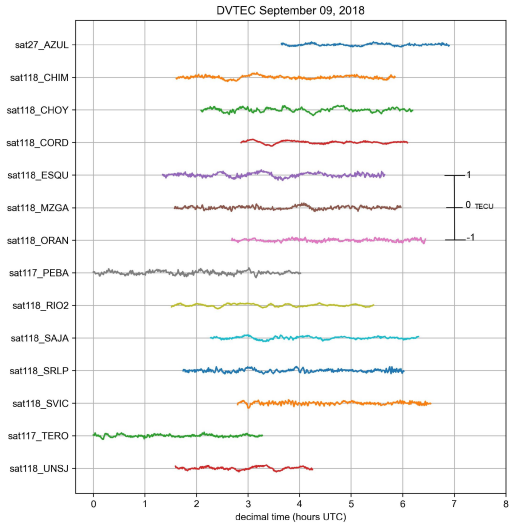

Figure 19. Reference day. Temporal variations of the differential vertical total electron content (DVTEC) of the 14 RAMSAC stations. On the y-axis, the stations are located 1 TECU apart. In the figure, a scale has been plotted for reference.

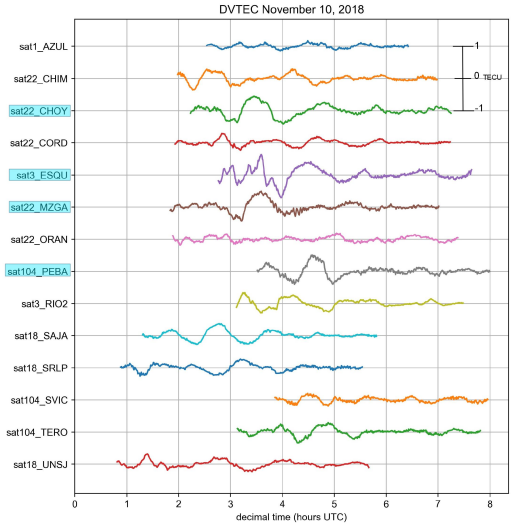

Figure 20. Day with AEA. Temporal variations of the differential vertical total electron content (DVTEC) of the 14 RAMSAC stations. On the y-axis, the stations are located 1 TECU apart. In the figure, a scale has been plotted for reference. The stations with the largest observed deviations in DVTEC are delineated.

The peak-to-peak DVTEC amplitudes for each station throughout the study period (00:00 UTC - 08:00 UTC) are shown in Figure 21 using multicolored diamonds, representing both the reference day (left panel) and the day with AEA (right panel). The lightning counts are also plotted using a 0.2° by 0.2° grid. The points where the maximum peak current of the different types of discharges occurred are marked with stars. On the reference day, the peak-to-peak DVTEC amplitudes measurements from all the stations collectively span from 0.01 to 0.44 TECU. Conversely, on the day with AEA, peak-to-peak DVTEC amplitudes ranged from 0.21 TECU to 1.35 TECU. This indicates an increase in amplitude across all stations, likely due to the presence of thunderstorms. It is worth noting that although stations CHOY and AZUL are located near the area of maximum discharge and peak current, they exhibit differences in their amplitude values. The same occurs with PEBA and SRLP, which are situated between the storms. Note that peak-to-peak DVTEC amplitudes ranging from 0.44 TECU to

Preprints (www.preprints.org) | NOT PEER-REVIEWED | Posted: 27 July 2023 doi:10.20944/preprints202307.1909.v1

0.67 TECU are predominant in the data.

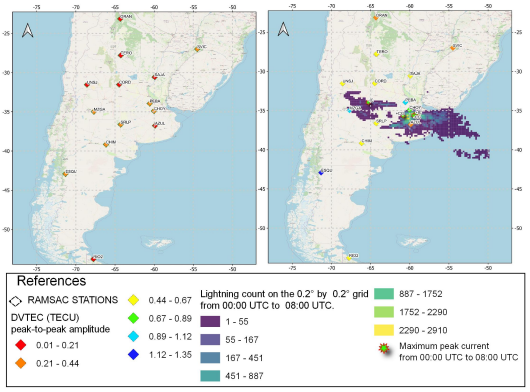

Figure 21. Maps of the 14 RAMSAC stations for the reference day (left image) and for the AEA day (right image). In the map of the day with AEA, we plot on the 0.2° by 0.2° grid the lightning count, and indicate with stars the locations of the highest peak currents for intracloud (IC) and Cloud-to-Ground (CG) discharges. In both maps, we represent with colored diamonds the peak-to-peak DVTEC amplitude values.

Table 3 shows the DVTEC peak-to-peak amplitude of the 14 analyzed stations for the entire study period (00:00 UTC - 08:00 UTC). In the table, we underlined station names whose peak-to-peak DVTEC increased by a factor of three or more, on the day of the storm, with respect to their reference peak-to-peak amplitude. These stations are ESQU, MZGA, PEBA, RIO2, SAJA and TERO. ESQU and RIO2 are situated south of the storm region; MZGA is within the storm zone, while PEBA, SAJA and TERO, are located north of the storm region.

By calculating the average peak-to-peak DVTEC amplitude of the 14 stations for the reference day, we obtained an average peak-to-peak amplitude of 0.23 TECU. On the other hand, the average peak-to-peak amplitude for the AEA day was 0.67 TECU. Comparing both results, we can see that on a stormy day the average peak-to-peak amplitude increases by a factor of 2.91 with respect to the average peak-to-peak amplitude of the non-stormy day.

Table 3. Peak-to-peak DVTEC amplitude of the 14 RAMSAC stations, for the reference and storm day in the whole study period (00:00 UTC - 08:00 UTC).

RAMSAC Stations	Peak-to-peak DVTEC Amplitude (TECU)	
	Day without AEA (Reference Day)	Day with AEA
AZUL	0.16	0.32
CHIM	0.27	0.66
CHOY	0.31	0.87
CORD	0.2	0.53
ESQU	.32	.35
MZGA	.26	.93
ORAN	0.19	0.37
PEBA	.29	.91
RIO2	.18	.63
SAJA	.2	.65
SRLP	0.23	0.53
SVIC	0.25	0.4
TERO	.21	.64
UNSJ	0.21	0.55

Preprints (www.preprints.org) | NOT PEER-REVIEWED | Posted: 27 July 2023 doi:10.20944/preprints202307.1909.v1

3.2.3. DVTEC Signal Period Analysis

In order to analyze the periods present in the DVTEC signal and its amplitude spectrum, the C-Morlet 1.5 wavelet transform was applied to five RAMSAC stations strategically selected in relation to the storm cells. Figure 22 shows the chosen stations (AZUL, MZGA, PEBA, SRLP and TERO) along with the DVTEC measurement paths of each satellite and the DVTEC peak-to-peak amplitudes during the entire study period (00:00 UTC - 08:00 UTC). In the map on the right, lightning is plotted on a 0.2° by 0.2° grid, and the locations where the maximum current peaks were recorded are indicated by stars. Observing the map on the right, we can notice that stations MZGA, PEBA and TERO present a predominantly longitudinal path of their satellites, while, stations AZUL and SRLP show a mostly latitudinal path, especially after 03:00 UTC.

Continuing with the analysis, we examine the DVTEC variation for the selected five stations on both, the day without and with AEA (refer to Figures 23 and 24). For the day without AEA, we observed DVTEC fluctuations with high-frequency content (Figure 23) and peak-to-peak DVTEC amplitudes ranging from 0.16 TECU to 0.29 TECU (see Table 3). On the other hand, for the day with AEA, we find DVTEC fluctuations with both low and high-frequency content (Figure 24) and higher peak-to-peak amplitudes ranging from 0.32 TECU to 0.93 TECU (Table 3). In addition, during the day with AEA, we observe that the stations tend to reach their maximum DVTEC variation between 03:00 UTC and 05:00 UTC. After that time, they tend to return to their nominal state.

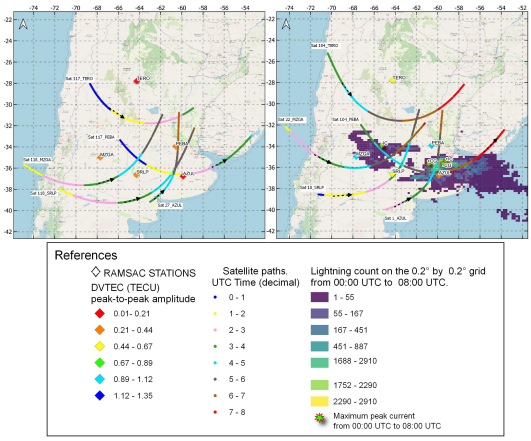

Figure 22. Maps of the 5 RAMSAC stations. The map on the left corresponds to September 9 and the one on the right to November 10, 2018. With colored dots, the trajectory in time followed by satellites 1, 18, 22, 27, 104, 117, and 118 are plotted. In both maps, we represent with colored diamonds the peak-to-peak DVTEC amplitude values. On the November 10 map, lightning count is plotted on the 0.2º by 0.2º grid, and locations, where the highest current peaks occurred for IntraCloud (IC) and Cloud-to-Ground (CG) discharges, are indicated with stars.

Preprints (www.preprints.org) | NOT PEER-REVIEWED | Posted: 27 July 2023 doi:10.20944/preprints202307.1909.v1

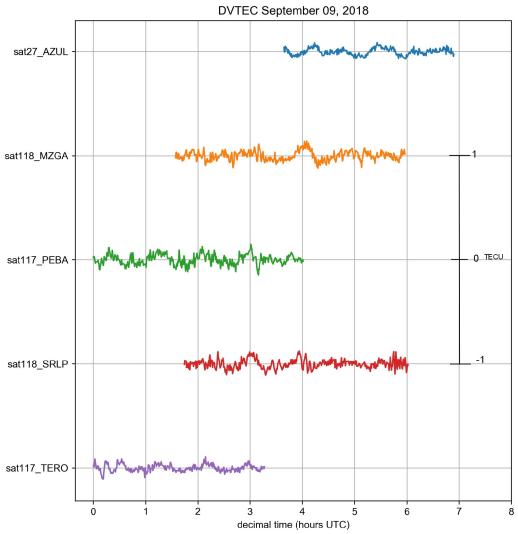

Figure 23. Reference day. Temporal variations of the differential vertical total electron content (DVTEC) of the 5 RAMSAC stations. On the y-axis, the stations are located 1 TECU apart. A scale has been plotted in the figure for reference.

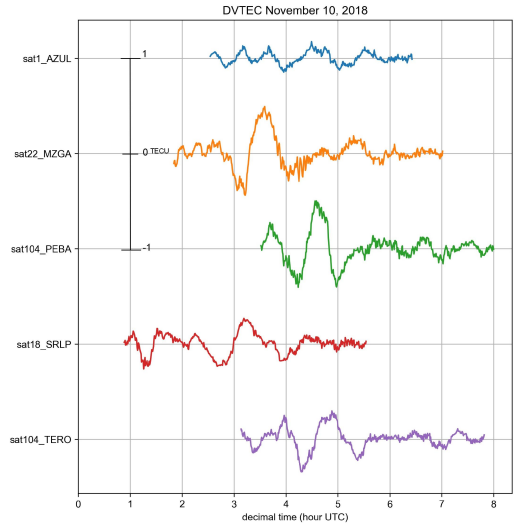

Figure 24. Day with AEA. Temporal variations of the differential vertical total electron content (DVTEC) of the 5 RAMSAC stations. On the y-axis, the stations are located 1 TECU apart. A scale has been plotted in the figure for reference.

We applied the wavelet transform to the data both for the day with the storm and for the day without the storm. Figures 25–29 show, for each station and GNSS satellite, the satellite path in decimal time (UTC), the peak-to-peak DVTEC amplitude (TECU), the lightning counts on the 0.2° by 0.2° grid, and the position of the maximum current peaks. In the lower-left panel, we have the DVTEC variation of the processed satellite data in decimal hours for both days. To the right of that panel, we show the continuous wavelet transform calculation with its confidence cone, which represents the 95% confidence in the result obtained within it. By observing the maps along with the temporal variation graphs of DVTEC (bottom-left panel), we find the highest DVTEC variations when:

- the AZUL station satellite (Figure 25) passes through the southeast storm. The maximum peak of variation is reached between about 03:50 UTC and 05:00 UTC, when it is passing through the area with the highest number of discharges.

Preprints (www.preprints.org) | NOT PEER-REVIEWED | Posted: 27 July 2023 doi:10.20944/preprints202307.1909.v1

- The satellite of the PEBA station (Figure 27) crosses the storm located in the central region. This occurs between 04:00 UTC and 05:00 UTC.
- The satellites of stations MZGA (Figure 26) and TERO (Figure 29) cross the area of the Andes Mountains. The maximum variations of MZGA and TERO occur between 03:00 UTC-04:00 UTC and between 04:00 UTC-05:00 UTC, respectively.
- The satellite of the SRLP station (Figure 28) crosses the Andes Mountains. In addition, we found the largest DVTEC variations when the satellite passed through the storm region. The first maximum occurs between 01:00 UTC and 02:00 UTC, and the second between 03:00 UTC and 04:00 UTC.

In these cases, we do not detect an at-a-glance relationship between the maximum peak currents and the maximum variations in the DVTEC of each station, since they occur at different times and locations.

Finally, as mentioned previously, Figures 25–29 present the wavelet transform of the five studied stations. Observing these figures, we see that for the day without AEA, the period of the DVTEC signal is less than 75 minutes, the peak-to-peak DVTEC amplitude is between [0.16 - 0.29] TECU and the spectral amplitude is between [0.1 - 0.2]. On the other hand, for the day with AEA, we find periods lower than 100 minutes, peak-to-peak DVTEC amplitude between [0.32-0.93] TECU, and spectral amplitudes between [0.25 - 1.4].

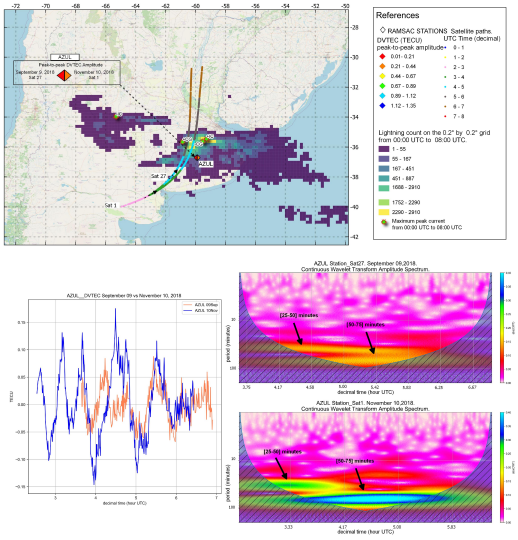

Figure 25. AZUL station, top panel: Station location with peak-to-peak DVTEC amplitude value plotted with colored diamonds; and satellite trajectory as a function of time for the reference day (September 9) and for the day with AEA (November 10). Lightning counts are plotted on the 0.2° by 0.2° grid, and the locations of the highest current peaks for IntraCloud (IC) and Cloud-to-Ground (CG) discharges are indicated with stars. Bottom panel: DVTEC time variations and periodogram (continuous wavelet transform) for both days are plotted. In the periodogram with arrows, the period obtained is marked.

Preprints (www.preprints.org) | NOT PEER-REVIEWED | Posted: 27 July 2023 doi:10.20944/preprints202307.1909.v1

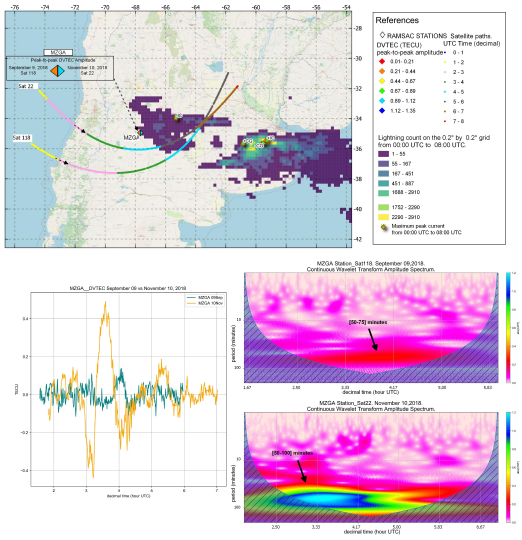

Figure 26. MZGA station, top panel: Station location with peak-to-peak DVTEC amplitude value plotted with colored diamonds; and satellite trajectory as a function of time for the reference day (September 9) and for the day with AEA (November 10). Lightning counts are plotted on the 0.2° by 0.2° grid, and the locations of the highest current peaks for IntraCloud (IC) and Cloud-to-Ground (CG) discharges are indicated with stars. Bottom panel: DVTEC time variations and periodogram (continuous wavelet transform) for both days are plotted. In the periodogram with arrows, the period obtained is marked.

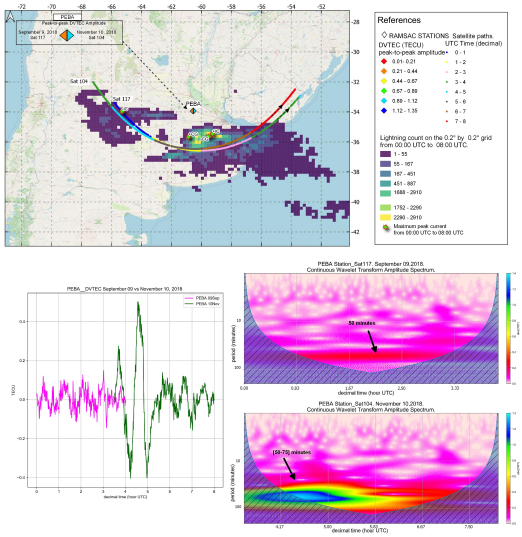

Figure 27. PEBA station, top panel: Station location with peak-to-peak DVTEC amplitude value plotted with colored diamonds; and satellite trajectory as a function of time for the reference day (September 9) and for the day with AEA (November 10). Lightning counts are plotted on the 0.2° by 0.2° grid, and the locations of the highest current peaks for IntraCloud (IC) and Cloud-to-Ground (CG) discharges are indicated with stars. Bottom panel: DVTEC time variations and periodogram (continuous wavelet transform) for both days are plotted. In the periodogram with arrows, the period obtained is marked.

Preprints (www.preprints.org) | NOT PEER-REVIEWED | Posted: 27 July 2023 doi:10.20944/preprints202307.1909.v1

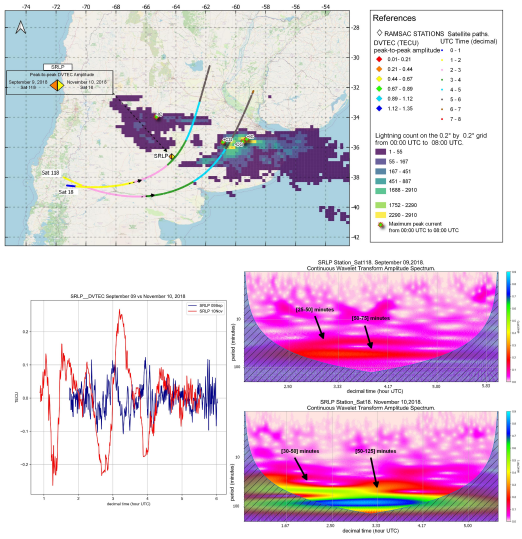

Figure 28. SRLP station, top panel: Station location with peak-to-peak DVTEC amplitude value plotted with colored diamonds; and satellite trajectory as a function of time for the reference day (September 9) and for the day with AEA (November 10). Lightning counts are plotted on the 0.2° by 0.2° grid, and the locations of the highest current peaks for IntraCloud (IC) and Cloud-to-Ground (CG) discharges are indicated with stars. Bottom panel: DVTEC time variations and periodogram (continuous wavelet transform) for both days are plotted. In the periodogram with arrows, the period obtained is marked.

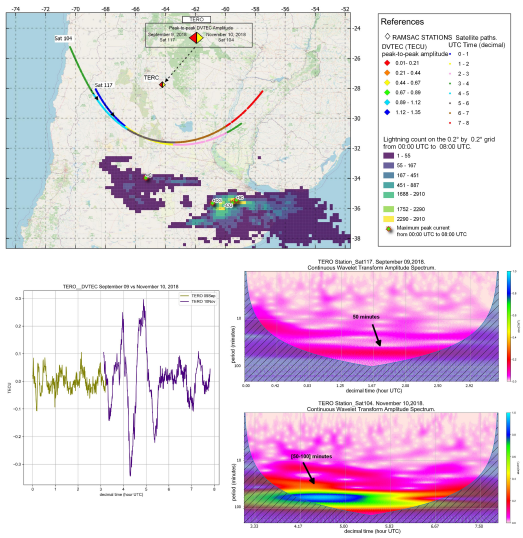

Figure 29. TERO station, top panel: Station location with peak-to-peak DVTEC amplitude value plotted with colored diamonds; and satellite trajectory as a function of time for the reference day (September 9) and for the day with AEA (November 10). Lightning counts are plotted on the 0.2° by 0.2° grid, and the locations of the highest current peaks for IntraCloud (IC) and Cloud-to-Ground (CG) discharges are indicated with stars. Bottom panel: DVTEC time variations and periodogram (continuous wavelet transform) for both days are plotted. In the periodogram with arrows, the period obtained is marked.

4. Discussion

During the period between 00:00 UTC and 08:00 UTC on November 10, 2018, there were two southeastward-moving storms in Argentina. While of the storms situated in the central region of the country, was in the developing stage, the other storm, located in the southeast region of the country, was already in the mature stage. The difference in their life stages led to the observation of a greater

Preprints (www.preprints.org) | NOT PEER-REVIEWED | Posted: 27 July 2023 doi:10.20944/preprints202307.1909.v1

number of discharges in the southeastern storm compared to the central storm, where lightning was found mainly at temperatures below -70°C, in the deep convective zones.

Based on the work of [3,5], gravity waves in TEC records from storms in the mid and low-latitude region, our analysis was divided into three periods to highlight the variability of the waves produced by the discharges. From this analysis, we found that:

1. In the period between 00:00 UTC and 02:40 UTC (21:00 LT - 23:40 LT), the RAMSAC stations showed DVTEC oscillations with peak-to-peak amplitude values of up to 0.67 TECU. Earth Networks lightning detection system reported peak current maxima of -219 kA for -CG and 181 kA for +CG. These maxima were located over the southeast of the storm, near the regions with the highest lightning count. Near these regions, the AGGO, AZUL, CHOY, LPGS, and PEBA stations showed peak-to-peak DVTEC amplitudes of up to 0.44 TECU. During this period, the storms were in their growth stage.
2. Between 02:40 UTC and 05:20 UTC (23:40 LT - 02:20 LT), RAMSAC stations showed oscillations in the DVTEC with peak-to-peak amplitude values of up to 1.35 TECU. The maximum peak currents were -214 kA for -CG and 211 kA for +CG, located above the storm located in the central region. Near the regions of maximum lightning count and maximum peak current, the AGGO, AZUL, CHOY, GVIL, MZAE, MZAU, MZGA, NUGA, RIO4, RUFI, and PEJO stations showed peak-to-peak DVTEC amplitudes of up to 1.12 TECU. During this period, the storms were in their development phase. In addition, during this time, the highest number of lightning flashes occurred and the highest peak-to-peak amplitudes were observed in the three analyzed zones.
3. In the period between 05:20 and 08:00 UTC (02:20 LT - 05:00 LT), RAMSAC stations showed DVTEC oscillations with peak-to-peak amplitude values of up to 0.67 TECU. In the southern region of Zone 3 (see Figure 17), the perturbations found cannot be directly attributed to the storms analyzed, since they are located in a region where a large number of gravitational waves were produced [48]. Moreover, current peaks in +CG of 322 kA and -CG of -267 kA were observed in this period. These peaks were located near the regions with the highest number of lightning flashes over the storm to the southeast. During this period, the storms showed a decrease in their atmospheric electrical activity.

In the different time periods, we obtained waveform structures in DVTEC with peak-to-peak amplitudes between [0.01 - 1.35] TECU. We could observe that in the time interval [02:40 - 05:20] UTC where the highest lightning count occurred, the highest peak-to-peak DVTEC amplitudes were observed.

To be sure if the wave-like structures observed in the DVTEC records are the result of storms, we worked with a base day (reference day), in which the geomagnetic activity was low and the electrical activity was null for the whole study period in Argentina. At this point, we worked only with 14 RAMSAC stations. Comparing the peak-to-peak DVTEC amplitude of the reference value with the peak-to-peak DVTEC amplitude of the day with AEA for the whole study period (00:00 UTC - 08:00 UTC), it was observed that the 14 stations presented disturbances due to storms. Out of these, the ESQU station had the highest DVTEC deviation levels, with a maximum peak-to-peak amplitude of 1.35 TECU. It was positioned to the southwest of the storm region, on the Andes Mountain. Additionally, two of the 14 stations (AZUL and CHOY) were situated above the storm located to the southeast, near the maximum peak current and lightning count. At these stations, peak-to-peak DVTEC amplitudes of 0.32 TECU and 0.87 TECU, respectively, were observed. Comparing these values with those obtained on a reference day, we observed that in both cases there was a greater than two-fold increase in peak-to-peak amplitude. Looking at the rest of the stations, we saw a 2.91-fold increase in the peak-to-peak amplitude of the DVTEC when thunderstorms were present (see Table 3). Therefore, we could say that the wavelet structures observed in the DVTEC signal were due to the studied storms .

Finally, five stations close to the region where the storms developed were analyzed for both days. From the wavelet analysis, variabilities with periods less than or equal to 100 minutes, spectral

 doi:10.20944/preprints202307.1909.v1

amplitudes up to 1.4 and peak-to-peak DVTEC amplitudes up to 0.93 TECU were obtained during the day with storm. Whereas, during the reference day, wavelets with periods less than 75 minutes, spectral amplitudes up to 0.2, and peak-to-peak DVTEC amplitude up to 0.29 TECU were observed.

5. Conclusions

To sum up, we performed an electrical characterization of the thunderstorms that took place in central Argentina on November 10 and observed their effect on the ionosphere. As a result, we obtained that the thunderstorm produced disturbances with periods less than or equal to 100 minutes and peak-to-peak DVTEC amplitudes up to 1.35 TECU. The results found are in agreement with the work of [49,50]. [49] found waves with periodicities around 60 minutes over West Africa; and [50], obtained an average period between 60 and 120 minutes for all regions of the world. These disturbances, known as atmospheric gravity waves, appear to be related to the lightning count. Indeed, when the highest lightning count occurred, the highest peak-to-peak amplitudes were obtained in the DVTEC.

Considering that CG discharges constitute 25% and IC discharges 75% of the atmospheric electrical activity ([45]), we can conclude that the results found in the percentage of discharges is as expected, since more than 70% of the discharges are of the IC type, mainly of negative polarity.

In thunderstorm conditions, DVTEC amplitudes between [0.1 - 1.4] TECU were obtained for the mid-latitude U.S. storms ([5]). For Chinese storms, corresponding to low latitudes, amplitudes between [0.2 - 0.8] TECU were obtained ([6]). While for the storms in Argentina developed in mid-latitudes, peak-to-peak amplitudes between [0.21 - 1.35] TECU were obtained.

When comparing the analyzed DVTEC signals, a progressive increase in instability was observed, especially in Zone 3. In particular, the southwest region of Zone 3 shows the most significant signal disturbances. It is worth mentioning that this specific zone is recognized for its frequent generation of gravitational waves ([48]). Therefore, the observed results cannot be attributed solely to the investigated storms.

In the period, 02:40-05:20 UTC, the highest peak-to-peak DVTEC amplitudes were obtained, and the highest lightning count was recorded. Therefore, does the high lightning count generate an increase in DVTEC amplitudes? Rahmani *et al.* [1] found a direct relationship between the increase in storm activity and DVTEC amplitudes. They found that the average amplitudes of disturbances on days with severe thunderstorms were 1.3 times greater than on days without lightning. In our case, the average peak-to-peak amplitude of the 14 stations on the day with thunderstorms was about 2.91 times higher than on the day without lightning activity.

Finally, the ABRA and ORAN stations are located more than 1000 km away from the storms. At these stations, we observed peak-to-peak DVTEC amplitude values higher than 0.21 TECU. Therefore, we detected disturbances more than 1000 km from the center of the storms. This distance is greater than that found in the work of [6], where they obtained perturbations 200-800 km from the storm center. This would indicate that gravitational waves can be found beyond the storm zone. According to [51] "This may occur since, under suitable conditions, gravity waves as they propagate upward become unstable at higher altitudes and may break up (at an altitude of about 100 km) into secondary waves ([12]) which continue to propagate upward, possibly modulating the E-region plasma distribution producing polarization electric fields that map the F-region ionosphere ([52])." Moreover, there are authors, such as [53], and [54], who suggest that these disturbances in the ionosphere may be due to vertical transport of electrostatic discharge ([4]). Others have suggested ([55]) that this may be caused by Transient Luminous Events (TLEs), which would induce fluctuations in the D region of the ionosphere ([4]).

Author Contributions: Conceptualization, C.I.V.A., M.G.N., A.M., M.P.N., and E.E.A.; methodology, C.I.V.A., M.G.N., A.M., M.P.N., and E.E.A.; software, C.I.V.A., A.M.,and M.P.N.; validation, C.I.V.A., M.G.N., A.M., M.P.N., and E.E.A.; formal analysis, C.I.V.A., M.G.N., A.M., M.P.N., and E.E.A.; investigation, C.I.V.A., M.G.N., A.M., M.P.N., and E.E.A.; resources, C.I.V.A., M.G.N., A.M., and M.P.N.; data curation, C.I.V.A., M.G.N.,and A.M.;

writing—original draft preparation, C.I.V.A., M.G.N., A.M., M.P.N., and E.E.A.; writing—review and editing, C.I.V.A., M.G.N., A.M., M.P.N., E.E.A., M.R., and F.R.; visualization, C.I.V.A., M.G.N., A.M., M.P.N., E.E.A., M.R., and F.R.; supervision, C.I.V.A., M.G.N., and E.E.A.; project administration, M.G.N., A.M.,and M.P.N.; funding acquisition, M.G.N., M.R., and F.R. All authors have read and agreed to the published version of the manuscript.

Funding: This research was funded by the Ministry of Defense grant number MINDEF PIDDEF 523 07/18: Environmental Risk Information Platform; and GeoRayos II and CITEDEF with the 524 GeoRayos II WEB Project and GINKGO 03 NAC 040/1. The APC was funded by HEIG-VD (Haute Ecole d'Ingénierie et de Gestion du Canton de Vaud) and EPFL (École polytechnique fédérale de Lausanne)

Data Availability Statement: TEC data available in a publicly accessible repository that does not issue DOIs. Publicly available datasets were analyzed in this study. This data can be found here: https://ri.conicet.gov.ar/handle/11336/201583 Atmospheric electrical activity data are available upon request due to restrictions, such as privacy. The data presented in this study can be obtained by contacting the Earth Networks support team to inquire about the process for acquiring the data, as it is not freely available.

Acknowledgments: This research was supported by the Ministry of Defense through MINDEF PIDDEF 07/18: Environmental Risk Information Platform; and GeoRayos II and CITEDEF with the GeoRayos II WEB Project and GINKGO 03 NAC 040/1. Constanza I. Villagrán Asiares is supported by the National Scientific and Technical Research Council (CONICET). Support was also provided by the Leading House for the Latin American Region Consolidation Grant of the University of Saint Gallen under Grant Agreement No. COG2230. In addition, the authors would like to thank Dr. Jeff Lapierre and Earth Networks (ENTLN) [29] for their support and for providing the lightning location data used in this work. We would also like to express our appreciation to all the participants of the RELAMPAGO campaign, who worked long hours to collect RELAMPAGO data. A special thank you to the campaign coordinators Paola Salio, and Stephen Nesbitt. We thank the National Science Foundation for their support of the RELAMPAGO project. Funding for the RELAMPAGO LMA was provided by the NOAA GOES- R Program, with additional support from the NASA Lightning Imaging Sensor (LIS) project. We are also grateful for the support provided by the Secretaría de Ciencia y Tecnología of the National University of Cordoba (UNC) and the Agencia Nacional de Promoción Científica (PICT 2019-2999). Lastly, the authors would also like to thank the International GNSS Service (IGS), the Crustal Dynamics Data Information Service (CDDIS), and the National Geographic Institute (IGN, Argentina).

Conflicts of Interest: The authors declare no conflict of interest.

Abbreviations

The following abbreviations are used in this manuscript:

AGWs	Atmospheric Gravity Waves
AEA	Atmospheric Electrical Activity
RELAMPAGO	Remote sensing of Electrification, Lightning, and Mesoscale/microscale Processes with Adaptive Ground Observations
CACTI	Clouds, Aerosols, and Complex Terrain Interactions
TEC	Total Electron Content
TECU	Total Electron Content Unit
GNSS	Global Navigation Satellite System
RAMSAC	Red Argentina de Monitorieo Satelital Continuo
ENTLN	Earth Networks Total Lightning Network
TLEs	Transient Luminous Events
CG	Cloud-to-Ground discharge
IC	Intra-Cloud discharge
TOA	Time-Of-Arrival
ABI	Advanced Baseline Imaging
GOES	Geostationary Operational Environmental Satellites
CDDIS	Crustal Dynamics Data Information System
BT	Brightness Temperature
IERSS	International Earth Rotation and Reference Systems Service
IGS	International GNSS Service
MAGGIA	Meteorología espacial, Atmósfera terrestre, Geodesia, Geodinámica, desarrollo de instrumentos y Astrometría

VTEC	Vertical Total Electron Content
STEC	Slant Total Electron Content
IPP	Ionospheric Piercing Point
DVTEC	Difference Vertical Total Electron Content
UTC	Universal Time Coordinated
LT	Local Time

References

1. Rahmani, Y.; Alizadeh, M.M.; Schuh, H.; Wickert, J.; Tsai, L.C. Probing vertical coupling effects of thunderstorms on lower ionosphere using GNSS data. *Advances in Space Research* **2020**, *66*, 1967–1976.
2. Chapman, S. The atmospheric height distribution of band-absorbed solar radiation. *Proceedings of the Physical Society (1926-1948)* **1939**, *51*, 93.
3. Lay, E.H.; Shao, X.M.; Kendrick, A.K.; Carrano, C.S. Ionospheric acoustic and gravity waves associated with midlatitude thunderstorms. *Journal of Geophysical Research: Space Physics* **2015**, *120*, 6010–6020.
4. Ogunsua, B.; Srivastava, A.; Bian, J.; Qie, X.; Wang, D.; Jiang, R.; Yang, J. Significant day-time ionospheric perturbation by thunderstorms along the West African and Congo sector of equatorial region. *Scientific reports* **2020**, *10*, 1–14.
5. Lay, E.H.; Shao, X.M.; Carrano, C.S. Variation in total electron content above large thunderstorms. *Geophysical Research Letters* **2013**, *40*, 1945–1949.
6. Liu, T.; Yu, Z.; Ding, Z.; Nie, W.; Xu, G. Observation of Ionospheric Gravity Waves Introduced by Thunderstorms in Low Latitudes China by GNSS. *Remote Sensing* **2021**, *13*, 4131.
7. Cheng, Z.; Cummer, S.A. Broadband VLF measurements of lightning-induced ionospheric perturbations. *Geophysical research letters* **2005**, *32*.
8. Vadas, S.; Liu, H.L. Numerical modeling of the large-scale neutral and plasma responses to the body forces created by the dissipation of gravity waves from 6 h of deep convection in Brazil. *Journal of Geophysical Research: Space Physics* **2013**, *118*, 2593–2617.
9. Vadas, S.L.; Fritts, D.C. Thermospheric responses to gravity waves arising from mesoscale convective complexes. *Journal of atmospheric and solar-terrestrial physics* **2004**, *66*, 781–804.
10. Walterscheid, R.; Schubert, G.; Brinkman, D. Acoustic waves in the upper mesosphere and lower thermosphere generated by deep tropical convection. *Journal of Geophysical Research: Space Physics* **2003**, *108*.
11. Zettergren, M.; Snively, J. Ionospheric signatures of acoustic waves generated by transient tropospheric forcing. *Geophysical Research Letters* **2013**, *40*, 5345–5349.
12. Snively, J.B.; Pasko, V.P. Breaking of thunderstorm-generated gravity waves as a source of short-period ducted waves at mesopause altitudes. *Geophysical Research Letters* **2003**, *30*.
13. Vadas, S.L.; Liu, H.l. Generation of large-scale gravity waves and neutral winds in the thermosphere from the dissipation of convectively generated gravity waves. *Journal of Geophysical Research: Space Physics* **2009**, *114*.
14. Asiares, C.I.V.; Nicora, M.G.; Meza, A.; Paula, M.; Avila, E.E.; et al. Relationship between the activity of thunderstorms and ionospheric oscillation during the RELAMPAGO Project. In Proceedings of the 2021 35th International Conference on Lightning Protection (ICLP) and XVI International Symposium on Lightning Protection (SIPDA). IEEE, 2021, Vol. 1, pp. 01–07.
15. Zipser, E.J.; Cecil, D.J.; Liu, C.; Nesbitt, S.W.; Yorty, D.P. Where are the most intense thunderstorms on Earth? *Bulletin of the American Meteorological Society* **2006**, *87*, 1057–1072.
16. Cecil, D.J.; Blankenship, C.B. Toward a global climatology of severe hailstorms as estimated by satellite passive microwave imagers. *Journal of Climate* **2012**, *25*, 687–703.
17. Piscitelli, F.M.; Ruiz, J.J.; Negri, P.; Salio, P. A multiyear radar-based climatology of supercell thunderstorms in central-eastern Argentina. *Atmospheric Research* **2022**, *277*, 106283.
18. Corrales, P.B.; Galligani, V.; Ruiz, J.; Sapucci, L.; Dillon, M.E.; Skabar, Y.G.; Sacco, M.; Schwartz, C.S.; Nesbitt, S.W. Hourly assimilation of different sources of observations including satellite radiances in a mesoscale convective system case during RELAMPAGO campaign. *Atmospheric Research* **2022**, p. 106456.

19. Bechis, H.; Galligani, V.; Imaz, M.A.; Cancelada, M.; Simone, I.; Piscitelli, F.; Maldonado, P.; Salio, P.; Nesbitt, S.W. A case study of a severe hailstorm in Mendoza, Argentina, during the RELAMPAGO-CACTI field campaign. *Atmospheric Research* **2022**, *271*, 106127.
20. Kumjian, M.R.; Gutierrez, R.; Soderholm, J.S.; Nesbitt, S.W.; Maldonado, P.; Luna, L.M.; Marquis, J.; Bowley, K.A.; Imaz, M.A.; Salio, P. Gargantuan hail in Argentina. *Bulletin of the American Meteorological Society* **2020**, *101*, E1241–E1258.
21. Arena, L.E. Granizos gigantes de Córdoba-Argentina I. El Coloso Victoria, 2020.
22. Nesbitt, S.W.; Salio, P.V.; Ávila, E.; Bitzer, P.; Carey, L.; Chandrasekar, V.; Deierling, W.; Dominguez, F.; Dillon, M.E.; Garcia, C.M.; et al. A storm safari in subtropical South America: Proyecto RELAMPAGO. *Bulletin of the American Meteorological Society* **2021**, *102*, E1621–E1644.
23. Varble, A.C.; Nesbitt, S.W.; Salio, P.; Hardin, J.C.; Bharadwaj, N.; Borque, P.; DeMott, P.J.; Feng, Z.; Hill, T.C.; Marquis, J.N.; et al. Utilizing a storm-generating hotspot to study convective cloud transitions: The CACTI experiment. *Bulletin of the American Meteorological Society* **2021**, *102*, E1597–E1620.
24. by the National Science Foundation., S. RELAMPAGO-CACTI campaign. `https://catalog.eol.ucar.edu/relampago`, 2018. Accessed June 2023.
25. SpaceWeatherLive is an initiative of Parsec vzw, a.B.n.p.o. "SpaceWeatherLive.Com | Real-Time Data and Plots Auroral Activity" n.d. `https://www.spaceweatherlive.com/`, 2008. Accessed June 2023.
26. Networks, E. Earth Networks Total Lightning Network. `https://www.earthnetworks.com/why-us/networks/lightning/`. Accessed June 2023.
27. Zhu, Y.; Stock, M.; Lapierre, J.; DiGangi, E. Upgrades of the Earth networks total lightning network in 2021. *Remote sensing* **2022**, *14*, 2209.
28. Networks, E. Earth Networks Total Lightning Network (ENTLN) Global Lightning Network. `https://ghrc.nsstc.nasa.gov/home/content/earth-networks-total-lightning-network-entln-global-lightning-network`. These data are not publicly available or free. Must contact the support team at Earth Networks to determine how to acquire the data. Accessed June 2023.
29. This page is maintained by University of Utah © 2020, Department of Atmospheric Science, U.o.U. GOES-16/17/18 on Amazon Download Page. `https://home.chpc.utah.edu/~u0553130/Brian_Blaylock/cgi-bin/goes16_download.cgi?source=aws&satellite=noaa-goes16&domain=F&product=ABI-L2-MCMIP&date=2018-12-14&hour=9`, 2020. Accessed June 2023.
30. Schmit, T.J.; Griffith, P.; Gunshor, M.M.; Daniels, J.M.; Goodman, S.J.; Lebair, W.J. A closer look at the ABI on the GOES-R series. *Bulletin of the American Meteorological Society* **2017**, *98*, 681–698.
31. Berrick, N.O.S. Crustal Dynamics Data Information System. `https://urs.earthdata.nasa.gov/oauth/authorize?client_id=gDQnv1IO0j9O2xXdwS8KMQ&response_type=code&redirect_uri=https%3A%2F%2Fcddis.nasa.gov%2Fproxyauth&state=aHR0cDovL2NkZGlzLm5hc2EuZ292L2FyY2hpdmUvZ25zcy8`. Accessed June 2023.
32. IGN. Instituto Geográfico Nacional. `https://www.ign.gob.ar/`. Accessed June 2023.
33. Adler, R.F.; Mack, R.A. Thunderstorm cloud top dynamics as inferred from satellite observations and a cloud top parcel model. *Journal of the atmospheric sciences* **1986**, *43*, 1945–1960.
34. Borque, P.; Vidal, L.; Rugna, M.; Lang, T.J.; Nicora, M.G.; Nesbitt, S.W. Distinctive signals in 1-min observations of overshooting tops and lightning activity in a severe supercell thunderstorm. *Journal of Geophysical Research: Atmospheres* **2020**, *125*, e2020JD032856.
35. Chris Vagasky, V.X. Total Lightning Statistics 2022. The Annual Lightning Report. `https://indd.adobe.com/view/d0591066-471e-41b9-83e1-4dc937aaeb96`, 2022. Accessed June 2023, pp 8.
36. Dach, R.; Lutz, S.; Walser, P.; Fridez, P. Bernese GNSS software version 5.2 **2015**.
37. Petit, G.; Luzum, B. The 2010 reference edition of the IERS conventions. In *Reference Frames for Applications in Geosciences*; Springer, 2013; pp. 57–61.
38. Letellier, T. Etude des ondes de marée sur les plateaux continentaux. PhD thesis, Toulouse 3, 2005.
39. van Dam, T.; Altamimi, Z.; Collilieux, X.; Ray, J. Topographically induced height errors in predicted atmospheric loading effects. *Journal of Geophysical Research: Solid Earth* **2010**, *115*.
40. UNLP, L.M.F. MAGGIA Laboratorio. `https://www.maggia.unlp.edu.ar/`. Accessed June 2023.
41. Meza, A.; Van Zele, M.A.; Rovira, M. Solar flare effect on the geomagnetic field and ionosphere. *Journal of atmospheric and solar-terrestrial physics* **2009**, *71*, 1322–1332.

42. Meza, A.; Bosch, G.; Natali, M.P.; Eylenstein, B. Ionospheric and geomagnetic response to the total solar eclipse on 21 August 2017. *Advances in Space Research* **2022**, *69*, 16–25.
43. Burrell, A.G.; Bonito, N.A.; Carrano, C.S. Total electron content processing from GPS observations to facilitate ionospheric modeling. *GPS solutions* **2009**, *13*, 83–95.
44. Fernández-Lavín, A.; Ovando-Shelley, E. Interpretación de señales usando transformadas wavelet continuas. In Proceedings of the Geotechnical Engineering in the XXI Century: Lessons learned and future challenges: Proceedings of the XVI Pan-American Conference on Soil Mechanics and Geotechnical Engineering (XVI PCSMGE), 17-20 November 2019, Cancun, Mexico. IOS Press, 2019, p. 138.
45. Nicora, M.G. Actividad eléctrica atmosférica en Sudamérica. PhD thesis, Universidad Nacional de La Plata, 2014.
46. DiGangi, E.; Lapierre, J.; Stock, M.; Hoekzema, M.; Cunha, B. Analyzing lightning characteristics in central and southern South America. *Electric Power Systems Research* **2022**, *213*, 108704.
47. Berger, K. Parameters of lightning flashes. *Electra* **1975**, *80*, 223–237.
48. Wu, D.L.; Eckermann, S.D. Global gravity wave variances from Aura MLS: Characteristics and interpretation. *Journal of the Atmospheric Sciences* **2008**, *65*, 3695–3718.
49. Blanc, E.; Farges, T.; Le Pichon, A.; Heinrich, P. Ten year observations of gravity waves from thunderstorms in western Africa. *Journal of Geophysical Research: Atmospheres* **2014**, *119*, 6409–6418.
50. Chowdhury, S.; Kundu, S.; Ghosh, S.; Sasmal, S.; Brundell, J.; Chakrabarti, S.K. Statistical study of global lightning activity and thunderstorm-induced gravity waves in the ionosphere using WWLLN and GNSS-TEC. *Journal of Geophysical Research: Space Physics* **2023**, p. e2022JA030516.
51. Kumar, S.; Chen, W.; Chen, M.; Liu, Z.; Singh, R. Thunderstorm-/lightning-induced ionospheric perturbation: An observation from equatorial and low-latitude stations around Hong Kong. *Journal of Geophysical Research: Space Physics* **2017**, *122*, 9032–9044.
52. Takahashi, H.; Taylor, M.J.; Pautet, P.D.; Medeiros, A.; Gobbi, D.; Wrasse, C.; Fechine, J.; Abdu, M.; Batista, I.; Paula, E.; et al. Simultaneous observation of ionospheric plasma bubbles and mesospheric gravity waves during the SpreadFEx Campaign. In Proceedings of the Annales Geophysicae. Copernicus GmbH, 2009, Vol. 27, pp. 1477–1487.
53. Davis, C.J.; Johnson, C.G. Lightning-induced intensification of the ionospheric sporadic E layer. *Nature* **2005**, *435*, 799–801.
54. Lay, E.; Shao, X.M. Multi-station probing of thunderstorm-generated D-layer fluctuations by using time-domain lightning waveforms. *Geophysical Research Letters* **2011**, *38*.
55. Qin, J.; Pasko, V.P.; McHarg, M.G.; Stenbaek-Nielsen, H.C. Plasma irregularities in the D-region ionosphere in association with sprite streamer initiation. *Nature communications* **2014**, *5*, 1–6.